Computational and Structural Biotechnology Journal 19 (2021) 1848–1862

COMPUTATIONAL AND STRUCTURAL BIOTECHNOLOGY JOURNAL

journal homepage: www.elsevier.com/locate/csbj

Temperature effect on the SARS-CoV-2: A molecular dynamics study of the spike homotrimeric glycoprotein

Didac Martí [a,b], Juan Torras [a,b,*], Oscar Bertran [c], Pau Turon [d,*], Carlos Alemán [a,b,e,*]

[a] Departament d'Enginyeria Química, EEBE, Universitat Politècnica de Catalunya, C/ Eduard Maristany, 10-14, Ed. I2, 08019 Barcelona, Spain
[b] Barcelona Research Center in Multiscale Science and Engineering, Universitat Politècnica de Catalunya, C/ Eduard Maristany, 10-14, 08019 Barcelona, Spain
[c] Departament de Física EETAC, Universitat Politècnica de Catalunya, c/ Esteve Terrades, 7, 08860 Castelldefels, Spain
[d] B. Braun Surgical, S.A.U. Carretera de Terrasa 121, 08191 Rubí (Barcelona), Spain
[e] Institute for Bioengineering of Catalonia (IBEC), The Barcelona Institute of Science and Technology, Baldiri Reixac 10-12, 08028 Barcelona Spain

ARTICLE INFO

Article history:
Received 8 February 2021
Received in revised form 27 March 2021
Accepted 29 March 2021
Available online 7 April 2021

Keywords:
Atomistic simulations
Receptor binding domain
Homotrimeric protein
Thermal inactivation
Virus spike

ABSTRACT

Rapid spread of SARS-CoV-2 virus have boosted the need of knowledge about inactivation mechanisms to minimize the impact of COVID-19 pandemic. Recent studies have shown that SARS-CoV-2 virus can be disabled by heating, the exposure time for total inactivation depending on the reached temperature (*e.g.* more than 45 min at 329 K or less than 5 min at 373 K. In spite of recent crystallographic structures, little is known about the molecular changes induced by the temperature. Here, we unravel the molecular basis of the effect of the temperature over the SARS-CoV-2 spike glycoprotein, which is a homotrimer with three identical monomers, by executing atomistic molecular dynamics (MD) simulations at 298, 310, 324, 338, 358 and 373 K. Furthermore, both the *closed down* and *open up* conformational states, which affect the accessibility of receptor binding domain, have been considered. Our results suggest that the spike homotrimer undergoes drastic changes in the topology of the hydrogen bonding interactions and important changes on the secondary structure of the receptor binding domain (RBD), while electrostatic interactions (*i.e.* salt bridges) are mainly preserved. The proposed inactivation mechanism has important implications for engineering new approaches to fight the SARS-CoV-2 coronavirus, as for example, cleaving or reorganizing the hydrogen bonds through chaotropic agents or nanoparticles with local surface resonant plasmon effect.

1. Introduction

The inactivation of SARS-CoV-2 has become a major objective as the spread of the beta coronavirus (β-CoV) has triggered a global health crisis with high social [1] and economic (global GDP contraction up to 6.9% for the year 2020) impact [2]. Virus inactivation can be achieved using different strategies based on chemical, biological and physical treatments. Biocide chemical agents and surfactants are frequently used to disinfect inanimate surfaces [3,4]. Furthermore, virus in culture media are deactivated by chemicals as TRIzol®, Formalin (formaldehyde) and β-propiolactone [5]. Biological treatments, in the format of vaccines, are the most effective to fight the virus in living organisms, even though their successful development is sometimes limited by a combination of economic factors, regulatory environment and the empirical nature of modern vaccine discovery [6–8]. Among physical treatments, cold plasma [9], far-UVC light [10] and membrane filtration [11] have been described to eliminate virus in surfaces, air and water, respectively, even though thermal inactivation is the most extensively used treatment when possible [5,12–17].

The stability of SARS-CoV-2 on different surfaces and temperatures was a source of concern from its beginning [18,19]. Focusing on the inactivation by temperature, it has been reported that SARS-CoV-2 was highly stable at low temperatures (*i.e.* 277 K up to 14 days) [20,21] but it is sensitive to heat. Indeed, several minimal inactivation temperatures, which are comprised between 329 K (45 min for inactivation) and 373 K (less than5 min for total inactivation [15]), have been reported [5,12–17]. On the other hand, the infectivity of SARS-CoV-2 in solution was strongly reduced (up to 100-fold), even though the virus remained similarly infective in surfaces at 277 and 303 K [21,22].

* Corresponding authors at: Departament d'Enginyeria Química, EEBE, Universitat Politècnica de Catalunya, C/ Eduard Maristany, 10-14, Ed. I2, 08019 Barcelona, Spain (J. Torras and C. Alemán).

E-mail addresses: joan.torras@upc.edu (J. Torras), pau.turon@bbraun.com (P. Turon), carlos.aleman@upc.edu (C. Alemán).

https://doi.org/10.1016/j.csbj.2021.03.037

Temperature is known to promote changes in the molecular structure of biomacromolecules (*i.e.* nucleic acids, proteins, lipids) until affecting their functionality. As part of natural evolution, such alterations have been used by microorganisms as an adaptation mechanism to environmental changes, for instance by variations in thermal labile hydrogen bonds (hereafter HBs) that connect the strands of nucleic acids and proteins [23]. In the particular case of proteins, temperature is known to induce variations of the secondary and tertiary structure, causing structural alterations that modify their stability and their role in regulating cellular processes, signal transduction and intrinsic enzymatic properties. However, the response of proteins to changes in the temperature conditions can be very different. For example, some proteins have high thermal stability while others can unfold or even denature at moderate temperature [24–26].

In this work we aim to unravel the effect of the temperature on the molecular structure of the SARS-CoV-2 spike glycoprotein, which is a homotrimer with three monomers with identical primary structure, named chain A, B and C. Coronaviruses use the spike to bind cellular receptors, triggering a cascade of events that leads to cell entry [27,28]. The spike protein is reported to bind the cellular receptor human angiotensin-converting enzyme 2 (ACE2) that mediates the fusion of the viral and cellular membrane and facilitates the virus introduction inside the cell [29]. Each spike monomer (180 kDa) contains 1273 amino acids (aa) and consists of a signal peptide (aa 1–13) and two subunits, named S1 (aa 14–685) and S2 (aa 686–1273), which are responsible for receptor binding and membrane fusion, respectively. The S1 subunit involves the N-terminal domain (NTD; aa 14–305) and the receptor binding domain (RBD; 319–541). The latter consists of a core region with 5 β-pleated sheets (β1, β2, β3, β4 and β7) organized in antiparallel model and the receptor-binding motif with two short β-pleated sheets (β5 and β6), loops and alpha helices (α4 and α5; [30]). A total of three cysteine residue pairs provide stability to the core and an additional cysteine residue pair helps in connecting the distal end of the receptor-binding motif [31]. The S2 subunit has a key role in the membrane fusion [32]. Thus, after the initial interaction of the RBD of the S1 subunit and the peptidase domain of ACE2, the fusion with the host cell membrane continues through the interaction between the heptad repeat 1 domain (HR1; aa 912–984), the central helix (CH; aa 985–1035), the connector domain (CD; aa 1076–1141), the heptad repeat 2 domain (HR2; aa 1163–1213) of S2 to form a helix bundle fusion core [33], which is extra stabilized by a short residue sequence (named fusion peptide of S2 or FP; aa 788–806; [34]). Furthermore, another important structural aspect of the SARS-CoV-2 spike is the identification of two states for the hinge-like conformation of the RBD of S1 from chain B [35,36]. These are: 1) the *closed down* state (Fig. 1a) in which the RBD of S1 covers the apical region of S2 near the C-terminus of HR1 (*i.e.* the receptor binding for interacting with ACE2 is buried); and 2) the *open up* (Fig. 1b) state in which the RBD is dissociated from the central axis of S2 and the NTD of S1 (*i.e.* the receptor binding motifs are exposed). Recently, a MD study of the S protein trimer exploring transition between closed and open states suggest the existence of a semi-open intermediate state for the SARS-CoV-2 spike, raising the possibility that ACE2 binding could take place in a semi-open intermediate state [37].

This study is focused on exploring the molecular structure of the spike glycoprotein of SARS-CoV-2 at different temperatures comprised within 298 K and 373 K using atomistic computer simulations. More specifically, atomistic Molecular Dynamics (MD) simulations have been conducted on the homotrimeric protein in aqueous solution considering both the closed down and the open up conformational states. MD is a computational tool that captures time-dependent conformational changes at various conditions by calculating inter-atomic forces through solvent Newton's second law. Moreover, this *in silico* methodology has been used to trace the atomic level contacts and interactions, which cannot be captured experimentally, and unveil a molecular mechanism for the virus inactivation. Such mechanism is intended to contribute to the development of new inactivation strategies by means of physical or chemical treatments specifically designed to disable such key interactions identified through the functional sites of the virus.

2. Methods

2.1. Construction of the molecular models

Cryoelectron microscopy structures of the homotrimeric spike glycoprotein of SARS-CoV-2 in the closed down (PDBid: 6vxx) and open up (PDBid: 6vyb) conformational states, solved at 2.80 Å and 3.20 Å, respectively [35], were taken from the Protein Data Bank and used to prepare the initial conformations. The missing residues (*i.e.* 44–55, 88, 89, 118–139, 147–159, 217–236, 417–429, 445–462, 476, 595–614, 651–653, 802–828, 1162–1175, 1236–1258, 1268–1280, 1292–1294, 1307–1309, 1338–1357, 1550–1556, 1562–1585, 1610–1616, 1716–1735, 1772–1783, 1923–1948, 2283–2296, 2360–2380, 2389–2401, 2459–2479, 2661–2263, 2671–2677, 2687–2706, 2837–2856, 2893–2905 and 3044–3071) were incorporated using the Modeler algorithm [38] implemented in the UCSF Chimera program [39] and the Z-DOPE (Discrete Optimized Protein Energy), statistical potential based for the choice of best model (*i.e.* that with the lowest Z-DOPE) for each conformational state, among the generated ones.

The homotrimeric protein models were then submerged in a previously equilibrated water box of 166.04 × 175.56 × 200.82 n m^3 for the closed down conformational state and of 161.05 × 183. 59 × 213.39 nm^3 for the open up one. Any water molecule that overlapped with any of the atoms belonging to the protein spike model was removed and, finally, a total of 154,517 and 168,125 water molecules were kept for the closed down and open up state, respectively. The models were completed by inserting randomly Na^+ and Cl^- ions until reaching a 0.15 M NaCl concentration to reproduce physiological conditions. Then, the two models were processes with the LEaP program [40] to add hydrogen atoms to the protein and to generate Amber topology files and coordinates files. Accordingly, the models used to represent the closed down and the open up states of the homotrimeric spike protein presented 516,706 and 558,601 explicit atoms, respectively.

2.2. Computational details

All simulations were performed using the AMBER 18 simulation suite [41]. Protein atoms were modeled using the Amber ff14SB force field [42], the glycan atoms included in the cryo-EM coordinates were modeled using the Glycam06 force field [43], and water atoms were modeled using the TIP3P force field [44]. The classical force fields can be used at high temperatures if the bond distance sampled does not oscillate much further beyond of the energetically minimum of its equilibrium bond distance. Indeed, many studies can be found in the protein denaturation literature using classical force fields at higher than physiological temperatures. [24,45–48]

Equilibration calculations were started by relaxing the protein regions filled with the UCSF Chimera program [39], which was achieved by applying the Limited-memory BroydenFletcher-Goldfarb-Shanno quasi-Newton algorithm methodology to the new added residues meanwhile the rest of the system was kept frozen. Next, the whole system was submitted to 2500 steps of full conjugate gradient minimization to relax conformational and structural tensions.

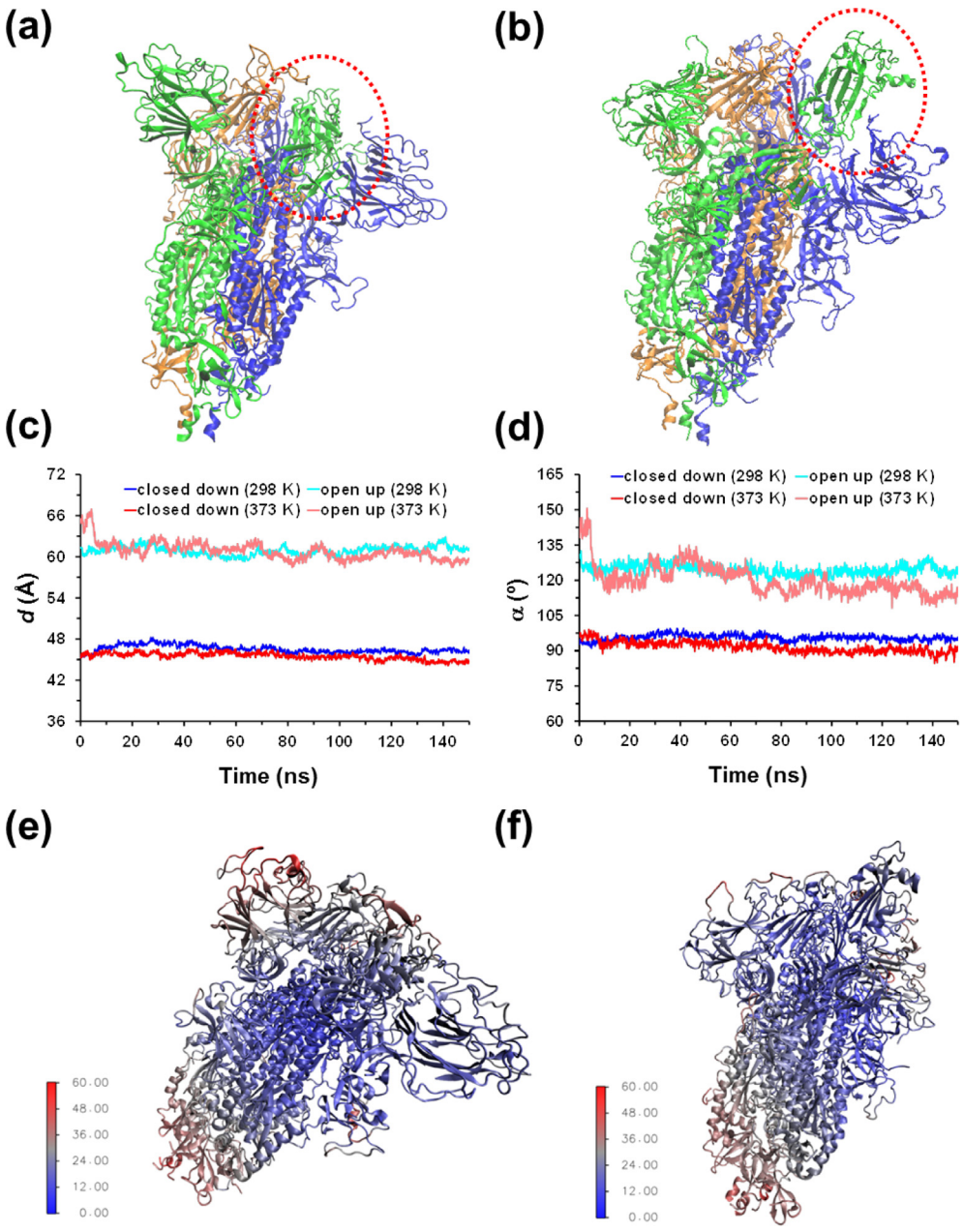

Fig. 1. (a) Closed down and (b) open up conformational states of the SARS-CoV-2 homotrimeric spike protein. The main difference between such two states is marked by the red dashed circle. For the MD simulations conducted at 298 and 373 K, temporal evolution of the geometric parameters used to identify the conformational states of the protein: (c) distance (*d*) between the centre of mass of the RBD from chain B to the centre of mass of three monomers; and (d) hinge angle (α) formed by the center of mass of the RBD of chain B, the center of mass of the rest of chain B, and the center of mass of the first residue after the RBD. For the (e) closed down and (f) open up states, color map structure of the spike protein at the end of the MD simulation at 373 K showing RMSD differences per residue between the end and initials snapshots. (For interpretation of the references to color in this figure legend, the reader is referred to the web version of this article.)

The Langevin dynamics method [49] was used to heat the system and to rapidly equilibrate its pressure and temperature. The relaxation times used for the coupling were 5 ps for both temperature and pressure. The temperature was increased from 0 K to 298 K using 60 ps simulation in the NVT ensemble, using an integration time step of 1 fs and keeping the pressure at 1.034 bar. Then, 1 ns in the NPT ensemble were conducted at 298 K to relax the structure and the density (integration step: 2 fs; pressure:1.034 bar). The last snapshot of this relaxation was used not only as starting point of the NPT production trajectory at 298 K but also as starting point of 0.25 ns NPT-MD simulation to bring the temperature to 310 K (integration step: 2 fs; pressure:1.034 bar). The last snapshot was used as starting point for the NPT production trajectory at such temperature and as starting point for the NPT-MD used to bring the temperature to 324 K. The same process was used to generate starting points for the production simulations 338, 358 and 373 K.

Production NVT-MD trajectories at 298, 310, 324, 338, 358 and 373 K were 150 ns each. Replica simulations were performed at all the indicated temperatures by changing the initial velocities. Accordingly, a total of 3.6 μs (150 ns × 2 conformational states × 6 temperatures × 2 replicas) were simulated for the studied system.

Non-bonding pairs list was updated every 10 steps. Periodic boundary conditions were applied using the nearest image convention and the atom pair cut-off distance used to compute the van

der Waals interactions was set at 10.0 Å. In order to avoid discontinuities in the potential energy function, non-bonding energy terms were forced to slowly converge to zero, by applying a smoothing factor from a distance of 12.0 Å. Beyond cut-off distance, electrostatic interactions were calculated by using Particle Mesh of Ewald [50].

3. Results

The atomic coordinates of the homotrimeric spike glycoprotein of SARS-CoV-2 in the closed down and open up conformational states were taken from the Protein Data Bank (PDB; entry 6vxx and 6vyb, respectively, from cryo-electron microscopy structures of the SARS-CoV-2 spike ectodomain trimer [35]. Missing protein segments were built using the UCSF Chimera program [39], which used the Modeller algorithm [38] to fill with the FASTA amino acids sequence while maintaining the crystallographic structure fixed. The different models generated for each conformational state were assessed using Z-DOPE (Discrete Optimized Protein Energy), a normalized atomic distance dependent statistical potential based on known protein structures. For each conformational state, the model scored with the lowest Z-DOPE, which was lower than −1 for both cases, was selected for MD simulations. After adding the hydrogen atoms and forming the disulphide bonds, the structures were solvated, thermalized and equilibrated using the protocol described in the Methods section (Supplementary Information). Finally, 150 ns long MD production runs in an NVT ensemble were conducted at 298, 310, 324, 338, 358 and 373 K using the Amber18 program [41]. In order to ensure the repeatability of the observed tendencies, replica simulations were performed at defined temperatures by changing the initial velocities. Accordingly, a total of 3.6 μs (150 ns × 2 conformational states × 6 temperatures × 2 replicas) were simulated for such a large system, which involved more than half million atoms.

The influence of the temperature on the closed down and open up states is quantitatively analyzed in Fig. 1c-d, which compares the temporal evolution of two different parameters calculated using data derived from simulations at 298 K and 373 K. These parameters, which have been defined to clearly differentiate between the two conformational states as well as to be able to identify the presence of intermediate states, are: 1) the distance (d) between the centre of mass of the RBD of chain B to the centre of mass of the three monomers; and 2) the hinge angle (α) formed by the center of mass of the RBD from chain B, the center of mass of the rest of chain B (*i.e.* excluding the RBD), and the center of mass of the first residue after the RBD. As it was expected, both parameters remain practically unaltered (less than 1.5% and 5.2% for d and α, respectively) along the MD trajectories at 298 K, the average values being d = 46.5 ± 0.5 Å and α = 95.6 ± 1.4° for the closed down and d = 60.9 ± 0.6 Å and α = 124.4 ± 2.2° for the open up. Interestingly, the average values obtained at 373 K, d = 45.5 ± 0.5 Å and α = 91.6 ± 2.3° for the closed down and d = 60.8 ± 1.3 Å and α = 120.2 ± 6.3° for the open up, are very similar compared to the previous one. Although the fluctuations around the average values are slightly higher at 373 K, especially for the open up conformation, results indicate the two states are unambiguously maintained during the whole simulations. Accordingly, the thermal energy gained at 373 K is not enough to destabilize the open up state and initiate a transition process towards the closed down. The same behavior was obtained for the rest of the studied temperatures (not shown).

Although detailed energetic analyses of the closed down and open up conformations are out of the scope of this work, we observed that the former state is stabilized with respect to the latter one, independently of the temperature. This stability order is in agreement with experimental observations [35,51,52]. Even though the two conformational states are maintained throughout all the trajectories, temperature affects the spike structure, causing changes that, after a certain threshold, cause the inactivation of the virus [5,12,17]. These changes are illustrated in Fig. 1e-f, which show the closed down and open up conformations obtained at the end of the MD trajectories at 373 K. As can be seen, the structures present significant differences to naked eye with respect to those shown in Fig. 1a-b, which were used as a starting point. These differences affect not only the secondary structure, but also the quaternary structure, which describes the interchain assembly between the three monomers. Thus, visual analysis of the open up conformation suggests that one of the monomers undergoes densification in certain regions due to structural deformations occurring at 373 K (blue monomer in Fig. 1f).

The influence of the temperature on the interchain assembly was analyzed by exploring the temporal evolution of the interchain distances (*i.e.* distance between two monomers), which was calculated as the distance between mass centres. Fig. 2a-b compares the A-B, B-C and A-C interchain distances at 298 and 373 K for the closed down and open up states. For the closed down state, the three interchain distances remain within the 32–34 Å interval, independently of the temperature. Instead, the open up state shows different interchain distances, even at room temperature. For example, at 298 K the values averaged over the last 75 ns of simulation are: d(A-B) = 37.1 ± 0.2 Å, d(B-C) = 35.6 ± 0.2 Å and d(A-C) = 31.9 ± 0.2 Å, reflecting that monomer A is closer to C than to B by ~ 9%. At 373 K, d(A-B) and d(B-C) converge to practically the same value (*i.e.* 35.4 ± 0.4 Å and 35.2 ± 0.3 Å, respectively), whereas d(A-C) decreases to 29.6 ± 0.2 Å. The latter represents a reduction of 16% with respect to the other two values and a reduction of 7% with respect to the distance at 298 K.

In order to ascertain if the effect on the assembly of the chains is associated to a change in the global shape of the individual monomers and of the whole homotrimeric construct, the dynamics of the radius of gyrations (R_g) was followed. The R_g for the individual chains does not exhibit abrupt changes when the temperature increases from 298 to 373 K (Fig. 2c-d). For the closed down state, the R_g is ~5 Å at the two analyzed temperatures. The R_g of chains A and C is ~44 Å for the open up state and slightly larger for chain B (~46 Å), even though the influence of the temperature in such values is very small (*e.g.* the R_g of monomer B averaged over the last 75 ns of the trajectory at 298 and 373 K is 46.2 ± 0.2 and 45.9 ± 0.2 Å, respectively). Similarly, although the effect of raising the temperature from 298 K to 373 K on the R_g of the whole assembly is slightly more pronounced for the open state (*i.e.* from 49.3 ± 0.1 Å to 48.6 ± 0.1 Å) than for the closed one (*i.e.* from 48.7 ± 0.1 Å to 48.5 ± 0.1 Å), changes do not reflect an important variation in shape of the supramolecular assembly (Fig. 2e-f).

All atom root mean square deviation (RMSD) and root mean square fluctuation (RMSF) plots determined from the MD trajectories for the closed down and open up conformational states at all the examined temperatures are illustrated in Fig. 3a-b and 3c-d, respectively. At the beginning of each trajectory, we observe a rapid increase in the RMSD, independently of the temperature and conformational state. However, the structure of the spike reaches a steady state after a few tenths of ns, even at the higher temperatures, corroborating that the simulated states are well equilibrated. The RMSDs recorded at 298, 310, 324 and 338 K are relative similar, around 4–5 Å, indicating moderate structural rearrangements, whereas the maximum values obtained at 358 and, especially, 373 K are consistent with more severe structural changes. Specifically, the RMSD values averaged over the last 50 ns of the simulations at 358 and 373 K are 6.8 and 8.3 Å, respectively, for the close down state and 8.8 and 12.7 Å, respectively, for the open up state.

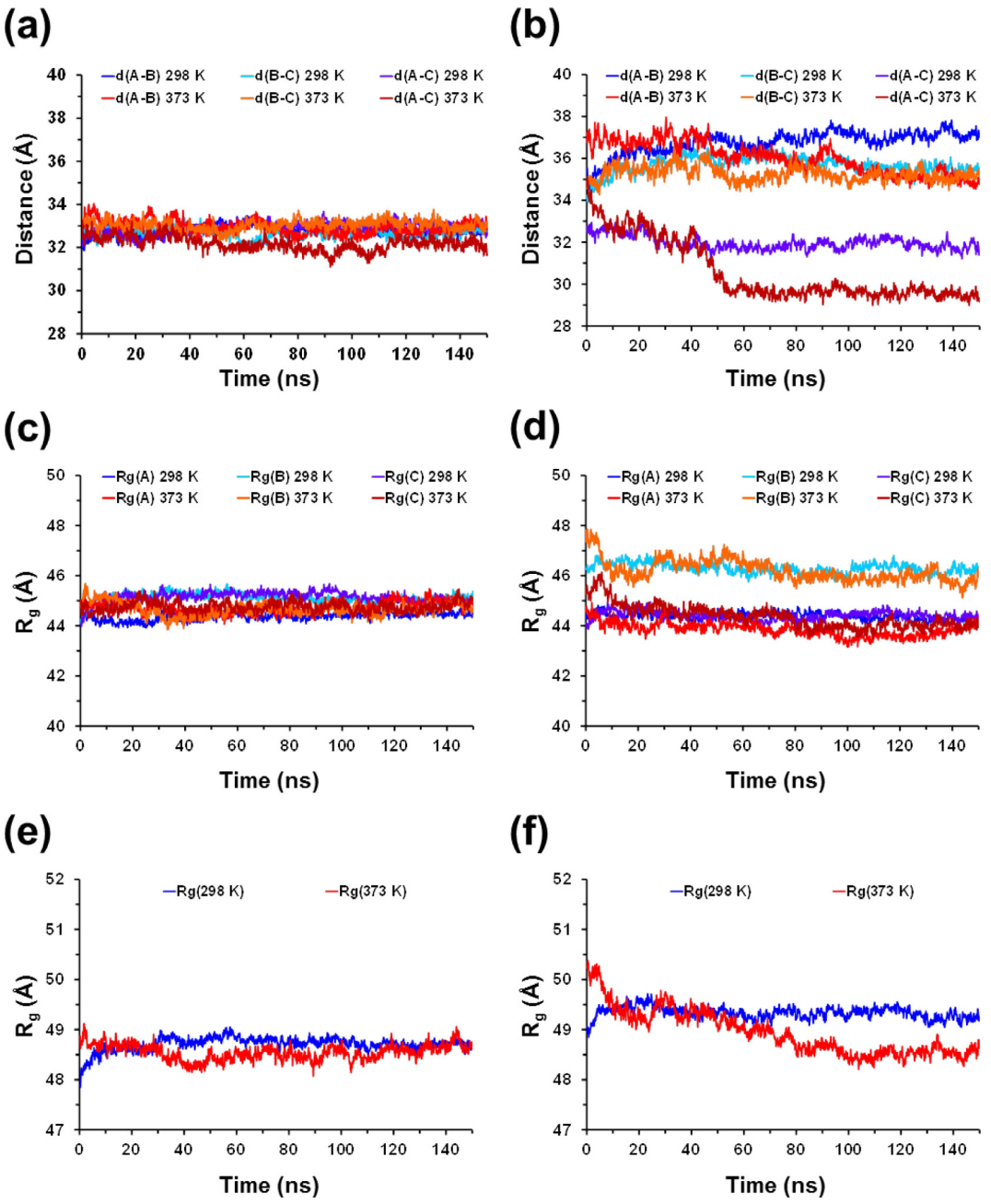

Fig. 2. For the (a, c, e) closed down and (b, d, f) open up states, temporal evolution at 298 and 373 K of: (a, b) the inter-chains distances calculated with respect to the centre of mass of each chain; (c, d) the radius of gyration of each chain; and (e, f) the radius of gyration of the whole supramolecular assembly formed by the three assembled chains.

In order to compare the overall flexibility of the two conformational states at the different temperatures, the RMSF was computed considering all atoms of each residue from the trimeric protein (Fig. 3c-d). As it was expected, fluctuations increase with temperature for the two conformational states. However, increments were relatively small for temperatures $\leq$ 338 K (*i.e.* average value grew from 1.7 / 1.9 Å (298 K) to 2.2 / 2.3 Å (338 K) for the closed down / open up states), increasing to values ~ 3 Å in average at 358 and 373 K. This feature is clearly illustrated in Fig. 3e-f, which represents the difference between the RMSFs calculated at 298 and 373 K considering all the atoms of each residue ($\Delta RMSF_{298\text{-}373}$).

Fig. 3e-f represents the difference between the RMSFs calculated at 298 and 373 K considering both all the atoms and only the C^{α} atom of each residue ($\Delta RMSF_{298\text{-}373}$). The profiles calculated using all atoms and the C^{α} atom are very similar, independently of the conformational state, indicating that the increment of temperature has a deep impact on the backbone organization and, therefore, on the secondary structure. Moreover, the effect is apparently different for the three chains of the homotrimer (split by dashed black lines in Fig. 3e-f). Thus, the thermal energy generated by heating from 298 to 373 K produces more fluctuations in the C chain for both the closed down and the open up states. In order to look in detail the effect of the temperature on the different domains for the two states, Fig. 4 compares the RMSF calculated at 298 and 373 K considering all atoms of each residue of chains A, B and C.

As is shown, the position of the following domains is indicated for each subunit of each chain: 1) the NTD and the RBD from the S1 subunit; and 2) the FD, the HR1, the CH and the CD from the S2

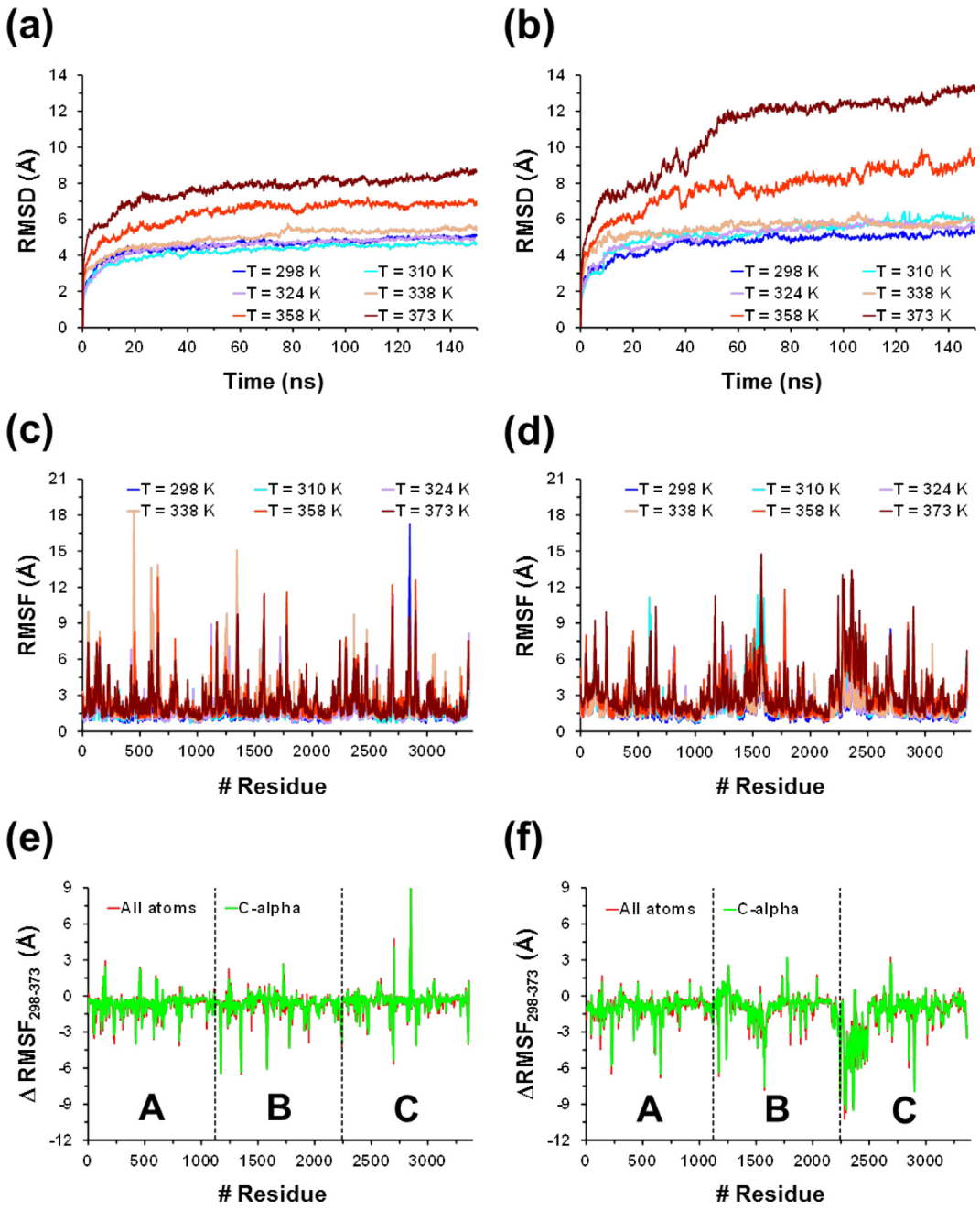

Fig. 3. For the (a, c, e) closed down and (b, d, f) open up states of SARS-CoV-2 homotrimeric spike protein: (a, b) Temporal evolution of the root mean square deviation (RMSD) and (c, d) root mean square fluctuation (RMSF) analyses calculated using all atoms for the MD simulations conducted at 298, 310, 324, 338, 358 and 373 K; and (e, f) difference between the RMSFs obtained at 298 and 373 K (ΔRMSF = RMSF(298 K) – RMSF(373 K) calculated using all the atoms (red profile) and the C^{α} atom (green profile) of each residue. The black dashed lines separate the three monomers (A, B and C) of the spike protein. (For interpretation of the references to color in this figure legend, the reader is referred to the web version of this article.)

subunit. For chain A, the S1 subunit is much more affected by the temperature than S2, reflecting that β-sheet rich domains, such as the NTD and the RBD, are more flexible than the helical rich domains located at S2. The flexibility of S1 is higher for the open up than for the closed down, as is evidenced by the fact that the RMSFs values reached at 373 K are, in general, higher for former state than for the latter one. Instead, the rigidity of S2 is similar for the two states with exception of HR1 domain, which shows large fluctuations at the central region for the closed down state. Inspection of the RMSFs achieved at intermediate temperatures indicates that the fluctuations reached by the S1 subunit of chain A increases progressively with heating. This is illustrated in Supplementary Fig. S1, which displays the RMSF calculated at 324 and 358 K.

The behavior shown by chain B is similar to that of chain A (Fig. 4 and Supplementary Fig. S1), the S1 subunit being much more influenced by the increase in temperature than S2. However, it should be noted that the fluctuations observed at 373 K in the NTD and RBD domains are much higher for the B chain than for the A one, indicating that in this case the flexibility of the S1 subunit is greater. This increase in the flexibility of S1 is particularly striking for the open state that reaches RMSF values close to 12 Å (NTD) or even higher (RBD). The effect of temperature in the open state is even more pronounced for the C chain, which shows a

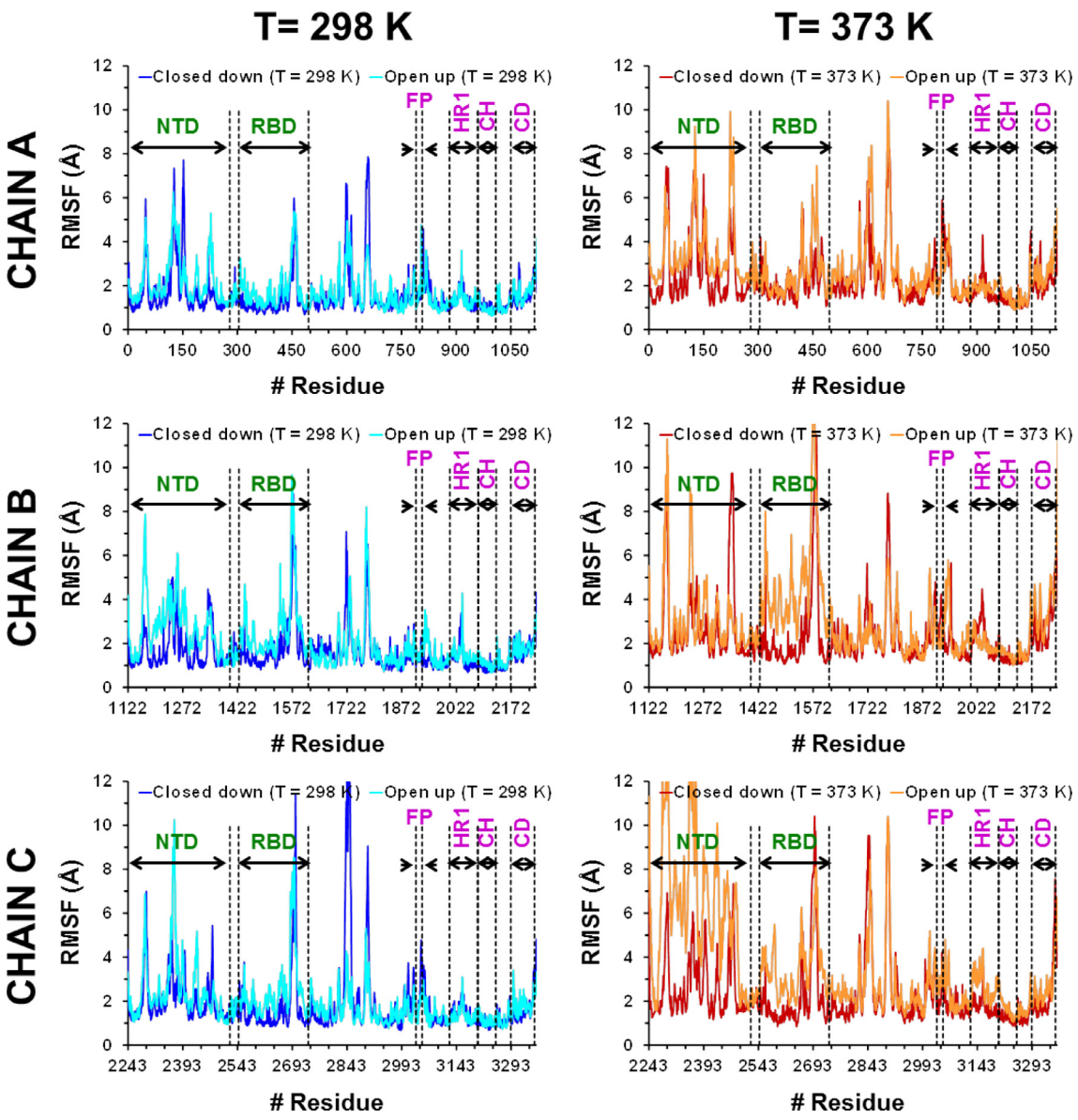

Fig. 4. For the three chains of the homotrimeric spike protein in the closed down and the open up states: root mean square fluctuation (RMSF) analyses calculated using all atoms for the molecular dynamics simulations at 298 K (left) and 373 K (right). The following domains are indicated in each graphic: the N-terminal and the receptor binding domain (NTD and RBD, respectively) from S1 subunit (marked in green), and the fusion peptide (FD), the heptapeptide repeat sequence 1 (HR1), the central helix (CH), the connector domain (CD) from S2 subunit (marked in violet). (For interpretation of the references to color in this figure legend, the reader is referred to the web version of this article.)

marked destabilization of the NTD at 373 K. It is worth noting that the thermal disruption of the NTD for the open up conformation also occurs at 358 K (see Supplementary Fig. S1 online), while the RSMF profiles of the two states at 324 K are similar to that calculated at 298 K.

In order to assess how the temperate affects the network of HBs, a detailed analysis on this specific interaction was conducted. The geometric parameters and the cut-off values used to define the D–H···A interaction (where A is an acceptor atom, D a donor heavy atom, and H a hydrogen atom) as HB are both the ∠DHA angle, which must be greater than 135°, and the D···A distance, that must be lower than 3.0 Å. Supplementary Fig. S2a compares the temporal evolution of the total amount of HBs existing and reorganized in the homotrimeric protein for the closed down and open up states at both 298 and 373 K. The profiles obtained at both temperatures are very similar, the average values for the closed down / open up conformations are 1566 ± 26 / 1535 ± 26 and 1538 ± 30 / 1557 ± 27 at 298 and 373 K, respectively. Moreover, intermediate temperatures exhibit a similar behavior (*e.g.* the amount of HBs at 338 K is 1570 ± 28 and 1560 ± 27 for the closed down and open up, respectively). Detailed analyses of the HBs involving residues from the RBD (Supplementary Fig. S2b) and NTB (Supplementary Fig. S2c) of chains A, B and C, which are the domains that exhibit the higher fluctuations at 373 K (Fig. 4), confirm that the change in terms of the number of HBs is not significant when the temperature increases from 298 to 373 K. For example, for the open up state the average number of HBs in the RBD of A, B and C chains is 72 ± 6 / 72 ± 6, 78 ± 7 / 80 ± 8 and 76 ± 6 / 74 ± 6 at 298 K / 373 K, respectively.

Fig. 5a shows the hydrogen bonding topology map at the end of the simulation at 373 K for both the closed down and open up states. Although a large number of HBs are detected for the two states, only a few ones involve the same residues of those existing at beginning of the simulations (marked by red dots). Thus, a large

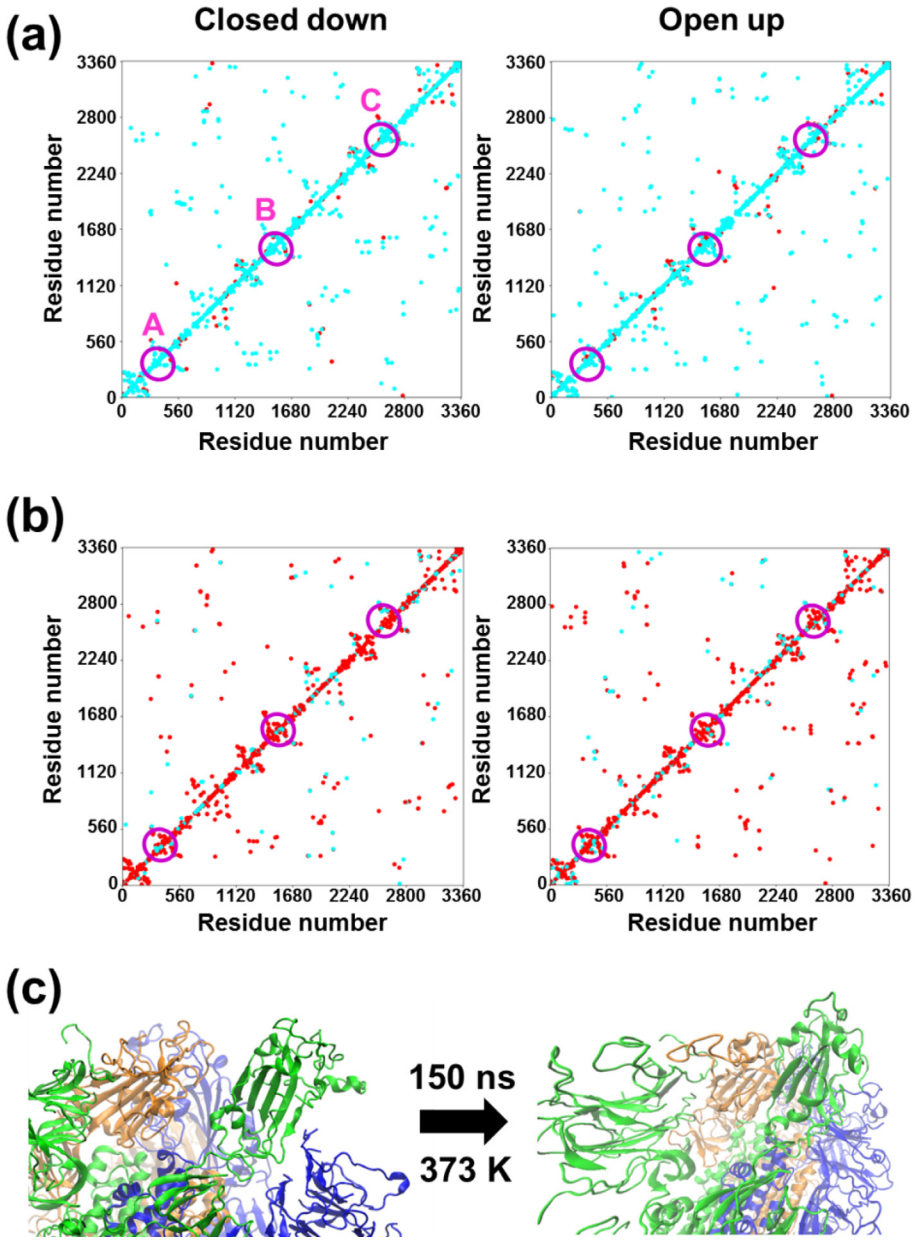

Fig. 5. Topology maps for the HBs found at the end of the simulations at (a) 373 K and (b) 298 K for the closed down and open up states. The *x*-and *y*-axes represent the residue number containing the hydrogen bonding donor and acceptor atoms, respectively. Red dots indicate HBs present at the starting structure that are maintained at the end of the simulation (*i.e.* the two residues involved in the HB do not change), while light blue dots correspond to the HBs that were not present at the starting conformation (*i.e.* the residue involving the hydrogen bonding donor and/or acceptor atoms change). The empty purple circles indicate the position of the RBD in the three chains of the homotrimer. (c) Representation of the region containing the RBD domains at the beginning and the end of the simulation for the open up state at 373 K. (For interpretation of the references to color in this figure legend, the reader is referred to the web version of this article.)

number of newly formed HBs implies a significant reorganization of the topological map (*i.e.* at the end of the simulation, the residue that involves the donor or acceptor atom in the HB is different from the one at the beginning). Conversely, original HBs are mostly preserved during the dynamics run at 298 K, as is shown in Fig. 5b for both studied conformational states. The HB topology through the 358 K trajectory remains roughly the same as 298 K. The changes induced by temperature in the RBD region of the open up state are illustrated in Fig. 5c and Supplementary Fig. S3, which compare the structure of such region in the initial and the last snapshot after 150 ns at 373 K and 298 K, respectively. As is shown, structural rearrangements are very significant at the highest temperature. Similar features are shown in Supplementary Fig. S4 for the closed down state.

The formation and temporal evolution of unspecific salt bridges (hereafter SBs), defined by an ion pair distance $\leq$ 4 Å, have been investigated considering the large amount of charged residues existing in the primary structure of the modelled protein (*i.e.* 49 Lys, 37 Arg, 15 His, 40 Glu and 53 Asp per monomer). SBs are electrostatic interactions in proteins that involve two charged groups, typically the cationic ammonium of a basic amino acid residue and the anionic carboxylate ion of an acidic amino acid residue. The amount of SBs as well as their geometric distribution (*i.e.* the topology map), are related with the protein rigidity and structural stability upon thermalization [53–56]. Indeed, SBs play a major role in structure of thermophilic proteins, which denature at a much higher temperature than regular proteins [55,56].

At 298 K the average amount of SBs is 178 ± 9 and 160 ± 7 for the closed down and open up states, respectively, increasing to 198 ± 10 and 188 ± 9, respectively, at 373 K (see Supplementary Fig. S5 online). Inspection of the topology maps for the SBs at the end of the simulations, which are displayed in Fig. 6, indicates that 268 (closed down) / 246 (open up) and 254 (closed down) / 224 (open up) of the initial interactions are retained after 150 ns at 298 and 373 K, respectively. Thus, around 73% / 66% and 69% / 61% of the initial SBs are preserved at 298 and 373 K, respectively. This fact suggests that such strong interactions, which are mainly of electrostatic nature, are responsible of the approximate conservation of the general shape of the spike protein.

The impact of the restrictions on the protein conformation has been further analyzed by considering distortions in the backbone φ,ψ-rotamers. For this purpose, φ,ψ-Ramachandran plots have been depicted for selected snapshots at the beginning (t = 0 ns), middle (t = 75 ns) and end (t = 150 ns) of the simulations. The approximate location and shape of the most favorable low-energy regions in this coordinate system is known to depend on the chemical structure of the residue. In this work, we have applied the classification proposed by Richardson and coworkers [57], according to which φ,ψ-maps of the following residues should be considered separately: 1) glycine (Gly) that is the most flexible residue due to the lack of side chain; 2) proline (Pro) with a singular cyclic structure that prohibits the rotation about the N—C^{α} bond and confines the φ torsion angle at around –60°; 3) residues preceding Pro (pre-Pro), which exhibit a very distinctive φ,ψ-distribution due to the steric restrictions imposed by the neighbor Pro [58]; and 4) the general case of the other 18 residues (hereafter, named General) that are largely influenced by the collision among main chain and C^{β} atoms. The energetically allowed φ,ψ-regions for General, Gly, Pro and pre-Pro residues are enclosed by the contours in the maps displayed in Supplementary Fig. S6 [57].

The φ,ψ-maps of General residues for the two states, calculated at 298 and 373 K, are shown in Supplementary Fig. S7a (t = 0 ns) and Fig. 7a (t = 75 and 150 ns). It is worth noting that the main part of such residues is located inside favored and allowed regions (blue dots within the contoured zones), while a small part is out but surrounding the allowed regions (red dots over the border or close to the contoured zones). The latter residues, which are found in a similar number for the two states, are modestly strained with a small energetic penalty with respect to the residues inside the favored regions. In addition, a few residues appear at forbidden areas with pronounced steric clashes (red dots over white regions), indicating highly strained conformations. These few disfavored residues

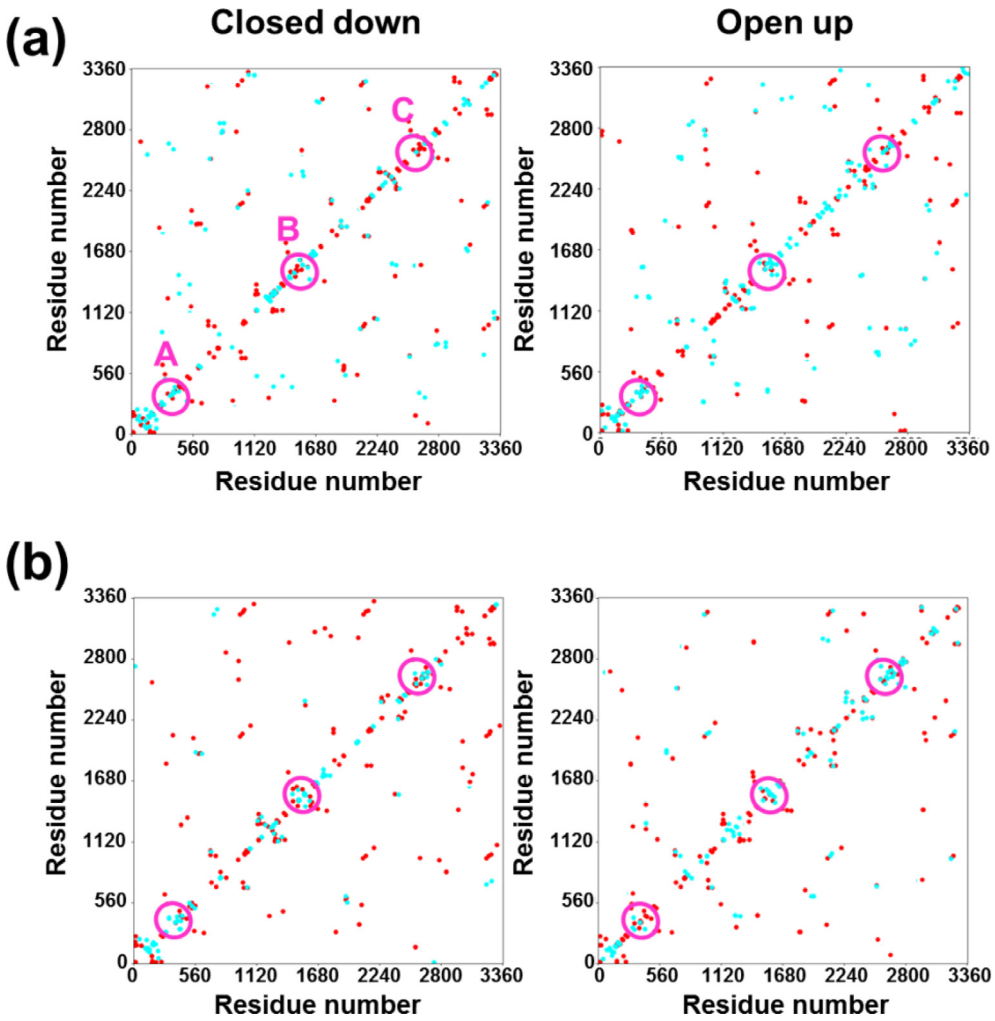

Fig. 6. Topology maps for the SBs found at the end of the simulations at (a) 373 K and (b) 298 K for the closed down and open up states. The *x*-and *y*-axes represent the residue number containing the positively charged and the negatively charged atoms, respectively. Red dots indicate SBs present at the starting structure that are maintained at the end of the simulation (*i.e.* the two residues involved in the SB do not change), while light blue dots correspond to the SBs that were not present at the starting conformation (*i.e.* the residue involving the positively or negatively charged atoms change). The empty purple circles indicate the position of the RBD in the three chains of the homotrimer. (For interpretation of the references to color in this figure legend, the reader is referred to the web version of this article.)

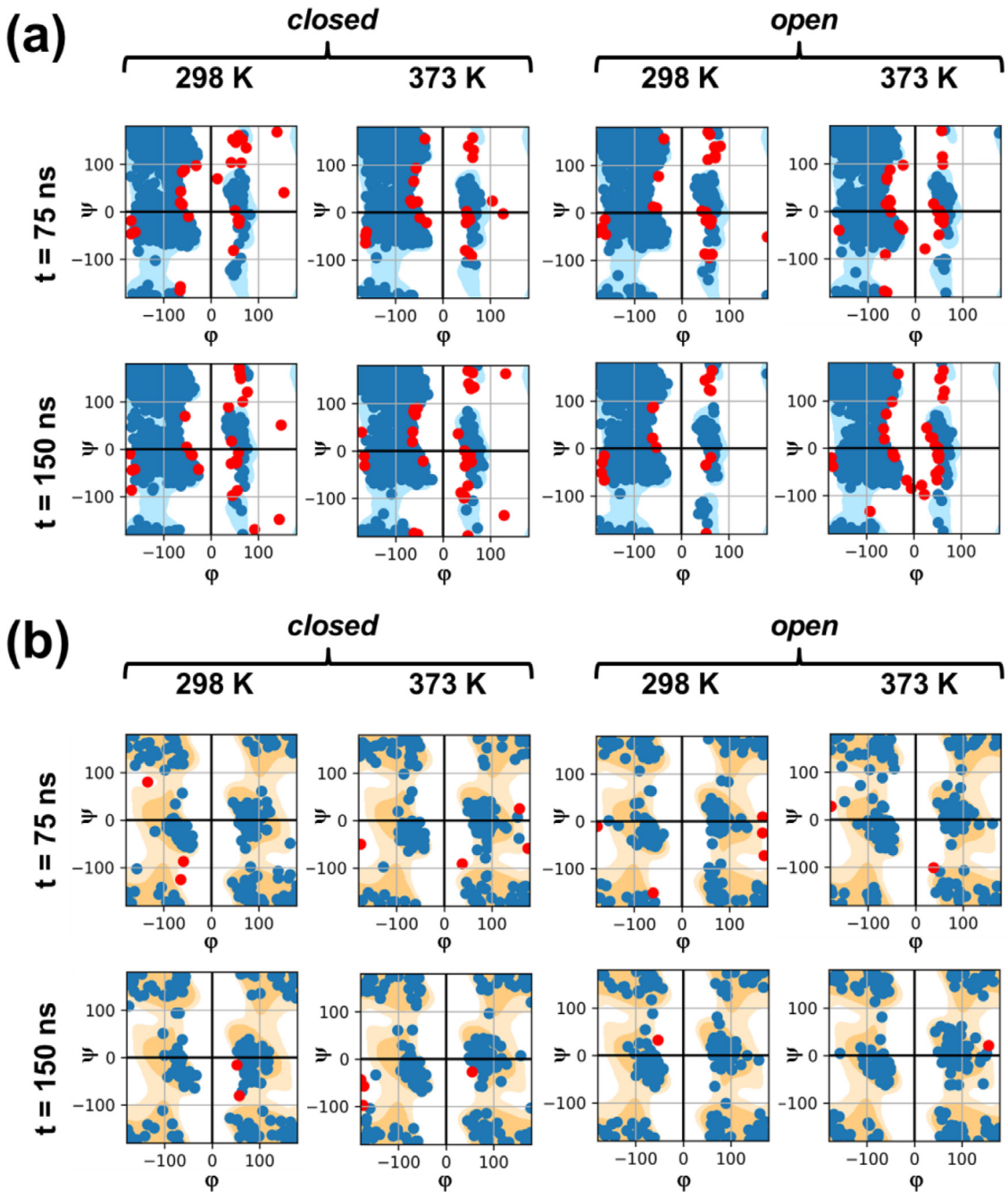

Fig. 7. Ramachandran maps showing the φ,ψ angle distributions for (a) General residues (non-Gly, non-Pro and non-prePro) and (b) flexible Gly residues as obtained from snapshots recorded in the middle (t = 75 ns) and at the end (t = 150 ns) of the trajectories conducted at 298 and 373 K for the closed down and open up conformations. Blue dots correspond to residues with allowed conformations (regions enclosed by the contours, see Supplementary Fig. S6 online), while red dots represent residues with strained (close to regions enclosed by the contours) or very strained (red dots over white regions) conformations. (For interpretation of the references to color in this figure legend, the reader is referred to the web version of this article.)

appear in the closed state even at the beginning of the simulation (see Supplementary Fig. S7a online), independently of the temperature, suggesting that they should be associated to the symmetric assembly of the three monomers rather to the heating process. Moreover, highly strained conformations are localized in chains B and C, as is proven in Supplementary Fig. S8 that compares the φ,ψ-maps for the three monomers at the end of the 298 and 373 K trajectories.

This effect is less pronounced for flexible Gly residues, as is shown in the φ,ψ-maps displayed in Supplementary Fig. S7b and Fig. 7b. Gly lacks of a side chain, making its φ,ψ values substantially less restricted than those related to other amino acids. Thus, the number of Gly residues localized in highly disfavored conformational regions (red dot over white regions) is very small, regardless of temperature. In this case, the increase in temperature from 298 to 373 K only causes a greater spreading of the blue dots inside the contoured regions, which is associated to the favored and allowed regions. This increment in the flexibility of Gly residue can be associated to structural deformations without significant energy penalties. A similar effect is observed for Pro and, especially, pre-Pro residues, as is shown in Supplementary Fig. S7c-d and S9. Although temperature induces the apparition of a few strained residues for both the closed down and open up states, this straining effect is much less pronounced than for General residues.

Besides, the apparition of strained pre-Pro residues is practically undetectable through all trajectories. It is worth noting that, in opposition to Gly, that is very flexible and able to accommodate in many different conformations, the behavior of Pro and pre-Pro has been attributed to the geometric restrictions imposed by the pyrrolidine ring.

Finally, the impact of temperature on the RBD of S1 subunit was studied by means of temperature induced conformational changes that might effect on the main RBD residue interactions map and thus impairs the potential bind with the human ACE2 receptor. Supplementary Fig. S10 and S11 show the RMSFs of the RBD interaction zone with the human ACE2 receptor for the open and closed conformation, respectively. The main displacements are observed in the monomer B for both starting conformations, *i.e.*, the open up and closed down. Less important displacements occur in the monomers A and C of the homotrimeric glycoprotein. According to experimental crystallographic work on the complex between the RBD and the human ACE2 receptor,[31] the highest concentration of HBs and SBs on the interface protein–protein are located in the residue range from 486 to 505 of the RBD. Interestingly, this region presents one of the highest flexibilities and fluctuations with temperature (Supporting Fig. S10 and S11). More specifically, two maximum fluctuations are observed around residues 444 to 450 and from 475 to 483 approximately, which correspond to regions where significant interactions of HB and SB with ACE2 were reported.[31]

In order to study the induced change in the secondary structure of RBD due to temperature, and more specifically in those key residues involved in the interaction with the human ACE2 receptor, the predominant RBD secondary structure along MD trajectory was compared at 298 and 373 K (Fig. 8). There is a great reorganization at the level of secondary structure throughout the whole RBD that extends to 51% of residue sequence in the open conformation and 29% in the closed conformation. It is also important to note that half of the key residues that are involved in HB and SB with human ACE2 receptor change their predominant secondary structure or there are significant changes in their populations as the temperature increases, while a large fluctuation in the RMSF is observed (Supplementary Fig. S10 and S11). Population breakdown of secondary structure of each one of the reported main interacting residues on the interface with ACE2 are shown in Supplementary Tables S1 and S2. More specifically, K417 and Y505 residues, which each one are involved in a SB formation with human ACE2 receptor, present an important change on the secondary structure population. Indeed, about 66% (K417) and 50% (Y505) of the snapshots along MD trajectory (last 75 ns) of the open up conformational state of the SARS-CoV-2 between 298 and 373 K have changed their secondary structure. Also, Y449 and N487, which are reported as important HBs on the interface with ACE2 also present a change of secondary structure on the 58 and 73% of the MD trajectory. This indicates an increase of protein denaturalization of this region with the temperature and an important effect on the potential binding affinity with human ACE2 receptor[59].

4. Discussion

The stabilization of the closed down conformation with respect to the open up, which is in agreement with experimental observations [35,51,52], has been attributed to the attractive inter-monomer interactions since the internal energy of each monomer is similar for the two states. Indeed, the interactions between RBD of a given monomer with the NTDs of neighboring monomers are favored in the closed down state compared to the open up and the interactions in the latter being truncated for the B chain. Moreover, the energy gap between the two states increases with the temperature due to the thermally-induced structural distortions that are more pronounced for the open up state. Instead, water-protein intermolecular interactions favor the open up conformation, which is obviously the consequence of the RBD exposition.

The narrow fluctuations of the A-B, B-C and A-C interchain distances found for the closed down state (Fig. 2a) indicate the homogeneous disposition of the three monomers is not perturbed by the temperature, which is consistent with the C3 symmetry imposed for the refinement of the cryo-electron microscopy data [60]. In opposition, the interchain distances obtained for the open up state (Fig. 2b) reflect not only that the A monomer is closer to C than to B but also that the temperature affects the interchain distances. Thus, the increment of temperature affects the packing of the trimers in the open up state, bringing closer two of the three chains. In spite of this change, the shape of the individual monomers and the whole homotrimer remain practically unaltered with the temperature, as deduced from the calculated R_g values (Fig. 2c-f).

Analysis of the temporal evolution of the RMSDs at different temperatures (Fig. 3a-b) reveals that the thermostability of the two examined conformational states is similar up to 338 K, the close down being more stable than the open up at higher temperatures. The RMSF profiles (Fig. 3c-d) reflect that atomic fluctuations associated to thermal instability of the closed down and open up states follow different patterns. More specifically, the higher fluctuations observed for the former state are more localized and less frequent than for the latter state, which exhibits important deviations at larger regions of the protein motifs. This feature is clearly illustrated by $\Delta RMSF_{298\text{-}373}$ values (Fig. 3e-f).

In general, the RMSFs profiles shown in Fig. 4 are fully consistent with cryo-electron microscopy observations of SARS-CoV-2 spike, which revealed considerable flexibility and dynamics in the S1 subunit [32,61]. In addition of the expected flexibility of RBD, which has been extensively investigated in this work by considering the closed down and open up states separately, the NTD flexibility suggested by cryo-electron microscopy structures is confirmed by MD simulations. Another region from S1 that deserves consideration is the one located between the RBD and the S2 subunit, which is usually subdivided in two structurally conserved subdomains identified as SD1 and SD2. These subdomains, especially SD1, act as a hinge point for RBD closed down–to–open up transitions and, therefore, are strongly affected by the breathing movements between the two states, which explain the relatively large fluctuations observed at all studied temperatures.

On the other hand, the preservation of the number of HBs with increasing temperature suggests that the glycoprotein spike of SARS-CoV-2 presents some kind of thermal stability, which at a first glance would not justify the inactivation of the virus by temperature. However, further understanding of the latter observation has been achieved by examining the changes in the topology of the hydrogen bonding network induced by the temperature. Thus, a large number of newly formed HBs are observed at 373 K. Conversely, native HBs were mostly preserved at 298 K for both studied conformational states through the dynamics runs. This difference explains the inactivation of the SARS-CoV-2 when rising the temperature. Although the largest change in the topology is achieved at 373 K, the observation of changes at lower temperatures is probably hindered by the limited length of the trajectories. More specifically, the total inactivation of the virus has been reported at 329 K after 45 min heating [5], which suggests a very slow kinetics for the conformational and topological changes related to hydrogen bonding reorganization.

Comparison of the topology maps at 298 and 373 K (Fig. 5a-b) suggests that, in general, the newly formed HBs involve residues that are relatively close to those involved in the native interactions. This feature is consistent with the fact that energy delivered

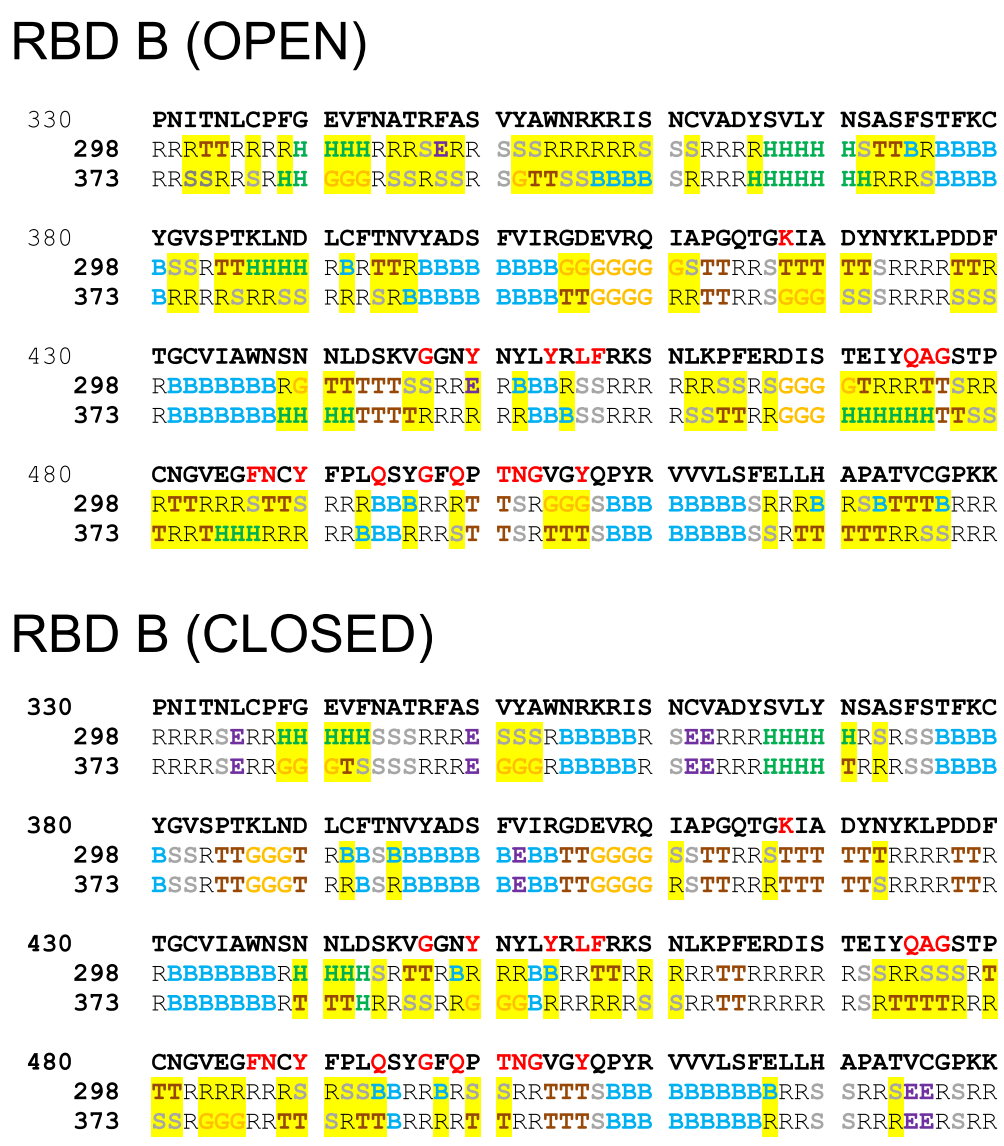

Fig. 8. Predominant secondary structure by residue along RBD sequence of monomer B in both open and close conformations. Results derived from last 75 ns of MD simulations of SARS-CoV-2 trimer at 298 and 373 K. Red letters refers to main residues interacting through HBs and SBs with human ACE2 receptor. All conformational differences are highlighted in yellow. Conformational keys: **E**, parallel β-sheet; **B**, anti-parallel β-sheet; **G**, 3–10 helix; **H**, α-helix; **I**, π(3–14)-helix; **T**, Turn; **S**, Bend; R, random coil. (For interpretation of the references to color in this figure legend, the reader is referred to the web version of this article.)

through heating induces changes in the secondary and, even, tertiary structure of the spike glycoprotein but not in its global shape or quaternary structure, as discussed above (Figs. 1 and 2). Considering the moderate strength of HBs (*i.e.* ideally, around −5 kcal/mol), the roughly retention of the shape at 373 K should be related to stronger noncovalent interactions. In fact, the average amount of SBs increases ~ 11% (closed down) / ~18% (open up) when the temperature rises from 298 to 373 K, supporting that SBs are responsible for the global shape retention observed at 373 K. Indeed, it is well known that SBs not only provide rigidity to thermophilic proteins [53–56] but also help to retain the global shape of thermostable membrane proteins when are subjected to temperatures similar to those considered in this work, as was experimentally observed in recent work [26].

Overall, analyses of the temperature influence on both HBs (weak directional interactions) and SBs (strong non-directional interactions) allow us to propose a molecular mechanism for the thermal inactivation of the virus. Such mechanism consists on differentiating the biological stability from the structural stability. The preservation of a large number of SBs and the formation of new ones upon increasing temperature are responsible of the structural stability in terms of protein global shape. Conversely, the deterioration of the hydrogen bonding network appears as the main reason for the functional inactivation of the virus upon heating. This mechanism is summarized in Fig. 9, which depicts the drastic conformational changes experienced by the NTD and RBD of chain B when temperature increases from 298 K to 373 K, whereas the overall shape of the spike is roughly preserved.

The loss of most of the initial hydrogen bonding interactions due to the increase in temperature facilitates new interactions with the surrounding active groups. However, the SBs structure, still preserved, restricts the degrees of freedom for establishing new interactions. In general, the geometric constrains imposed by SBs limit the formation of new HBs among residues located relatively close to those that make functional the infective form. The strength of SBs restricts the flexibility of the protein domains, limiting the molecular fluctuations and, consequently, the range of residues that can be involved in suitable directional interactions, involving only those that are spatially close. Such specific interac-

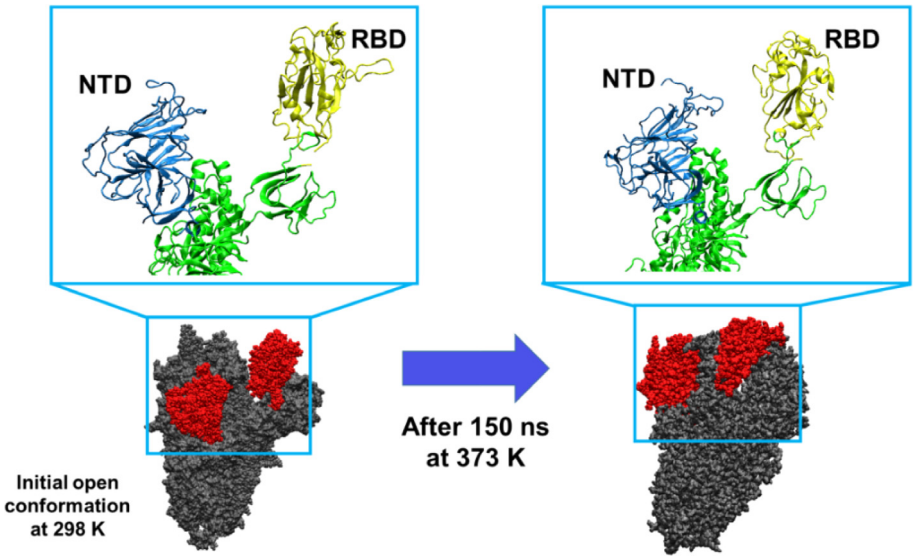

Fig. 9. The increase of temperature produces drastic conformational changes in the S1 subunit of the heterotrimeric spike protein (explicitly sketched for chain B), affecting also the orientation of the regions containing the NTD and RBD domains (in red). These changes are proposed to inactivate the virus by modifying the binding area to the cellular receptor, even though the general shape of the whole proteins remains roughly unaltered (grey). (For interpretation of the references to color in this figure legend, the reader is referred to the web version of this article.)

tions result in the new HB network that defines the topology of the inactive form of the virus.

It is worth noting that in the main region of interaction (RBD) of the spike glycoprotein of SARS-CoV-2 with the human ACE2 receptor, secondary structure changes between 298 and 373 K lead to a large structural reorganization. Changes in the secondary structure of up to 51% of the residue sequence are reported in this work for the open up conformational state compared to 29% of residues for the closed down state of monomer B (Fig. 8). When considering only those RBD residues of the homotrimer that are critical for the interaction with the RBD-ACE2 receptor, an important fluctuation with temperature was observed (Supplementary Fig. S10 and S11) that lead to relevant changes in their secondary structure populations, therefore, the residues involved mainly in the hydrogen bonding network and the SBs of the interface with ACE2 are affected (Supplementary Table S1 and S2). Taking into account the role that these residues play in the interface with the receptor,[31] it is possible to foresee a significant loss of affinity due to the RBD denaturation detected by temperature. Interestingly, these changes are more important for the open up state of monomer B, which is considered as the main active conformational state interacting with the receptor, rather than the closed down state. [60]

The φ,ψ-maps displayed in Fig. 7 and Supplementary Fig. S7-S9 are fully consistent with the mechanism proposed in Fig. 9. Thus, the General residues, which are able to form HBs and SBs, experience not only the largest conformational changes but also, in some cases, adopt strained conformations, as suggested by the topology maps calculated for those interactions. Such findings, open new avenues to develop strategies to inactivate the virus, by targeting specific areas of the homotrimer in order to misbalance, remodel or cleave the HBs that make the virus functional (*i.e.* by using chaotropic agents or surfactants that make feasible the disruption of hydrogen and SBs). Furthermore, it allows the development of active devices able to deliver energy that can cleave and reorganize HBs, for instance, through ultrasounds, irradiation or by using nanoparticles as nanosources of heat able to induce a local increment of temperature by using the local surface resonant plasmon effect, a phenomenon that occurs when light interacts with matter at specific wavelengths. Experimental work is currently ongoing using gold nanoparticles able to be heated as nanosources of heat when they are illuminated with a specific wavelength. This methodology can be used to kill tumoral cells [62–64] by transferring heat to target cells, as well as to inactivate bacteria [65] and virus (*e.g.* SARS-CoV-2).[66] The effectiveness of such local thermal treatment could be increased by controlling the intensity of the light source, the irradiation time lapse and the functionalization of nanoparticle designed to maximize the interaction with the virus areas where the higher number of HBs is exposed.

In summary, our results suggest that temperature induces conformational changes on the S1 subunit of the spike glycoprotein of SARS-CoV-2 that remodel the internal hydrogen bonding structure and affect specially to the secondary structure of RBD. However, the impact of temperature, even at 373 K, is not strong enough to induce a significant modification in the global shape of the spike. Those conformational changes, are much more pronounced in the state where the binding domain is accessible and the virus is infective (open up state) than when the binding domain is retracted (closed down state). This effect has been associated to a drastic modification in the hydrogen bonding topology, which particularly affects the recognition functionality of the receptor binding domain. Such network reorganization is triggered by the energy delivered through heat that allows the massive cleavage and remodeling of a significant amount of hydrogens bonds. Conversely, the SBs topology remains much less altered, allowing to maintain the main structure that defines the shape of the spike. The deep knowledge about such inactivation mechanism facilitates the development of new strategies intended to inactivate the virus through the destruction or modification of such HBs by chaotropic agents and surfactants or through physical treatments able to selectively target such labile HB structures.

CRediT authorship contribution statement

Didac Martí: Investigation, Formal analysis, Methodology, Software, Validation, Visualization. **Juan Torras:** Conceptualization, Investigation, Supervision, Funding acquisition, Methodology, Validation, Writing - review & editing. **Oscar Bertran:** Methodology, Software. **Pau Turon:** Conceptualization, Formal analysis, Funding

acquisition, Writing - original draft, Writing - review & editing. **Carlos Alemán:** Conceptualization, Formal analysis, Funding acquisition, Visualization, Writing - original draft, Writing - review & editing.

Declaration of Competing Interest

The authors declare that they have no known competing financial interests or personal relationships that could have appeared to influence the work reported in this paper.

Acknowledgements

J.T. acknowledges "Partnership for Advanced Computing in Europe" (PRACE) for awarding us access to Joliot-Curie at GENCI@CEA (Irene), France, through the "PRACE support to mitigate impact of COVID-19 pandemic" call. CA Acknowledges the Agència de Gestió d'Ajuts Universitaris i de Recerca (2017SGR359) and B. Braun Surgical, S.A.U. for financial support. Support for the research of C.A. was received through the prize "ICREA Academia" for excellence in research funded by the Generalitat de Catalunya.

Appendix A. Supplementary data

Supplementary data to this article can be found online at https://doi.org/10.1016/j.csbj.2021.03.037.

References

[1] WHO. Weekly operational update on COVID-19 - 8 February 2022021 [February 8th]; Available from: https://www.who.int/docs/default-source/coronaviruse/wou_2021_8february_cleared.pdf.
[2] World_Bank. Global Economic Prospects. Washington, DC2020.
[3] Kampf G, Todt D, Pfaender S, Steinmann E. Persistence of coronaviruses on inanimate surfaces and their inactivation with biocidal agents. J Hosp Infect 2020;104(3):246–51.
[4] Smith ML, Gandolfi S, Coshall PM, Rahman PKSM. Biosurfactants: A Covid-19 Perspective. Front Microbiol. [Perspective]. 2020 2020-June-09;11(1341).
[5] Jureka AS, Silvas JA, Basler CF. Propagation, inactivation, and safety testing of SARS-CoV-2. Viruses 2020;12(6):622.
[6] Loomis RJ, Johnson PR. Emerging vaccine technologies. Vaccines 2015;3(2):429–47.
[7] Rappuoli R, Pizza M, Del Giudice G, De Gregorio E. Vaccines, new opportunities for a new society. Proc Natl Acad Sci 2014;111(34):12288–93.
[8] Tannock GA, Kim H, Xue L. Why are vaccines against many human viral diseases still unavailable; an historic perspective?. J Med Virol 2020;92(2):129–38.
[9] Filipić A, Gutierrez-Aguirre I, Primc G, Mozetič M, Dobnik D. Cold plasma, a new hope in the field of virus inactivation. Trends Biotechnol 2020;38(11):1278–91.
[10] Buonanno M, Welch D, Shuryak I, Brenner DJ. Far-UVC light (222 nm) efficiently and safely inactivates airborne human coronaviruses. Sci Rep 2020;10(1):10285.
[11] Shirasaki N, Matsushita T, Matsui Y, Marubayashi T, Murai K. Investigation of enteric adenovirus and poliovirus removal by coagulation processes and suitability of bacteriophages MS2 and φX174 as surrogates for those viruses. Sci Total Environ 2016;563–564:29–39.
[12] Abraham JP, Plourde BD, Cheng L. Using heat to kill SARS-CoV-2. Rev Med Virol 2020;30(5):e2115.
[13] Cimolai N. Features of enteric disease from human coronaviruses: Implications for COVID-19. J Med Virol 2020;92(10):1834–44.
[14] Hu X, An T, Situ B, Hu Y, Ou Z, Li Q, et al. Heat inactivation of serum interferes with the immunoanalysis of antibodies to SARS-CoV-2. J Clin Lab Anal 2020;34(9):e23411.
[15] Kampf G, Voss A, Scheithauer S. Inactivation of coronaviruses by heat. J Hosp Infect 2020;105(2):348–9.
[16] Pastorino B, Touret F, Gilles M, de Lamballerie X, Charrel RN. Heat inactivation of different types of SARS-CoV-2 samples: what protocols for biosafety, molecular detection and serological diagnostics?. Viruses 2020;12(7):735.
[17] Yap TF, Liu Z, Shveda RA, Preston DJ. A predictive model of the temperature-dependent inactivation of coronaviruses. Appl Phys Lett 2020;117(6):060601.
[18] van Doremalen N, Bushmaker T, Morris DH, Holbrook MG, Gamble A, Williamson BN, et al. Aerosol and Surface Stability of SARS-CoV-2 as Compared with SARS-CoV-1. N Engl J Med 2020;382(16):1564–7.
[19] Yuan S, Jiang S-C, Li Z-L. Do humidity and temperature impact the spread of the novel coronavirus?. Front. Public Health [Opinion] 2020;8(240).
[20] Chin AWH, Chu JTS, Perera MRA, Hui KPY, Yen H-L, Chan MCW, et al. Stability of SARS-CoV-2 in different environmental conditions. The Lancet Microbe 2020;1(1):e10.
[21] Harbourt DE, Haddow AD, Piper AE, Bloomfield H, Kearney BJ, Fetterer D, et al. Modeling the stability of severe acute respiratory syndrome coronavirus 2 (SARS-CoV-2) on skin, currency, and clothing. PLoS NeglTrop Dis 2020;14(11):e0008831.
[22] Kratzel A, Steiner S, Todt D, V'Kovski P, Brueggemann Y, Steinmann J, et al. Temperature-dependent surface stability of SARS-CoV-2. J Infect 2020;81(3):452–82.
[23] Sengupta P, Garrity P. Sensing temperature. Curr Biol. 2013 2013/04/22/;23(8):R304-R7.
[24] Dong Y-w, Liao M-l, Meng X-l, Somero GN. Structural flexibility and protein adaptation to temperature: Molecular dynamics analysis of malate dehydrogenases of marine molluscs. Proc Natl Acad Sci 2018;115(6):1274–9.
[25] Julió Plana L, Nadra AD, Estrin DA, Luque FJ, Capece L. Thermal stability of globins: implications of flexibility and heme coordination studied by molecular dynamics simulations. J Chem Inf Model 2019;59(1):441–52.
[26] Lopes-Rodrigues M, Puiggalí-Jou A, Martí-Balleste D, del Valle LJ, Michaux C, Perpète EA, et al. Thermomechanical response of a representative porin for biomimetics. ACS Omega 2018;3(7):7856–67.
[27] Song W, Gui M, Wang X, Xiang Y. Cryo-EM structure of the SARS coronavirus spike glycoprotein in complex with its host cell receptor ACE2. PLoS Pathog 2018;14(8):e1007236.
[28] Zhou P, Yang X-L, Wang X-G, Hu B, Zhang L, Zhang W, et al. A pneumonia outbreak associated with a new coronavirus of probable bat origin. Nature 2020;579(7798):270–3.
[29] Ou X, Liu Y, Lei X, Li P, Mi D, Ren L, et al. Characterization of spike glycoprotein of SARS-CoV-2 on virus entry and its immune cross-reactivity with SARS-CoV. Nat Commun 2020;11(1):1620.
[30] Shang J, Ye G, Shi K, Wan Y, Luo C, Aihara H, et al. Structural basis of receptor recognition by SARS-CoV-2. Nature 2020;581(7807):221–4.
[31] Lan J, Ge J, Yu J, Shan S, Zhou H, Fan S, et al. Structure of the SARS-CoV-2 spike receptor-binding domain bound to the ACE2 receptor. Nature 2020;581(7807):215–20.
[32] Kirchdoerfer RN, Cottrell CA, Wang N, Pallesen J, Yassine HM, Turner HL, et al. Pre-fusion structure of a human coronavirus spike protein. Nature 2016;531(7592):118–21.
[33] Bosch BJ, Martina BEE, van der Zee R, Lepault J, Haijema BJ, Versluis C, et al. Severe acute respiratory syndrome coronavirus (SARS-CoV) infection inhibition using spike protein heptad repeat-derived peptides. Proc Natl Acad Sci U S A 2004;101(22):8455–60.
[34] Xia S, Liu M, Wang C, Xu W, Lan Q, Feng S, et al. Inhibition of SARS-CoV-2 (previously 2019-nCoV) infection by a highly potent pan-coronavirus fusion inhibitor targeting its spike protein that harbors a high capacity to mediate membrane fusion. Cell Res 2020;30(4):343–5.
[35] Walls AC, Park Y-J, Tortorici MA, Wall A, McGuire AT, Veesler D. Structure, function, and antigenicity of the SARS-CoV-2 spike glycoprotein. Cell 2020;181(2):281–92.
[36] Wrapp D, Wang N, Corbett KS, Goldsmith JA, Hsieh C-L, Abiona O, et al. Cryo-EM structure of the 2019-nCoV spike in the prefusion conformation. Science 2020;367(6483):1260–3.
[37] Gur M, Taka E, Yilmaz SZ, Kilinc C, Aktas U, Golcuk M. Conformational transition of SARS-CoV-2 spike glycoprotein between its closed and open states. J Chem Phys 2020;153(7):075101.
[38] Webb B, Sali A. Comparative protein structure modeling using MODELLER. Curr Protoc Protein Sci 2016;54(1):5.6.1–5.6.37.
[39] Pettersen EF, Goddard TD, Huang CC, Couch GS, Greenblatt DM, Meng EC, et al. UCSF Chimera—a visualization system for exploratory research and analysis. J Comput Chem 2004;25(13):1605–12.
[40] Case DA, I TECII, Darden T, Gohlke H, Luo R, Merz KM, et al. The Amber biomolecular simulation programs. J Comput Chem. 2005;26(16):1668-88.
[41] Case DA, Ben-Shalom IY, Brozell SR, Cerutti DS, Cheatham-III TE, Cruzeiro VWD, et al. AMBER 2018. San Francisco: University of California; 2018.
[42] Maier JA, Martinez C, Kasavajhala K, Wickstrom L, Hauser KE, Simmerling C. ff14SB: improving the accuracy of protein side chain and backbone parameters from ff99SB. J Chem Theory Comput 2015;11(8):3696–713.
[43] Kirschner KN, Yongye AB, Tschampel SM, González-Outeiriño J, Daniels CR, Foley BL, et al. GLYCAM06: a generalizable biomolecular force field. Carbohydrates. J Comput Chem 2008;29(4):622–55.
[44] Jorgensen WL, Chandrasekhar J, Madura JD, Impey RW, Klein ML. Comparison of simple potential functions for simulating liquid water. J Chem Phys 1983;79(2):926–35.
[45] Caflisch A, Karplus M. Molecular dynamics simulation of protein denaturation: solvation of the hydrophobic cores and secondary structure of barnase. Proc Natl Acad Sci 1994;91(5):1746–50.
[46] Bennion BJ, Daggett V. The molecular basis for the chemical denaturation of proteins by urea. Proc Natl Acad Sci 2003;100(9):5142–7.
[47] Yang C, Jang S, Pak Y. A fully atomistic computer simulation study of cold denaturation of a β-hairpin. Nat Commun 2014;5(1):5773.
[48] Paul S, Paul S. Molecular insights into the role of aqueous trehalose solution on temperature-induced protein denaturation. J Phys Chem B 2015;119(4):1598–610.
[49] Izaguirre JA, Catarello DP, Wozniak JM, Skeel RD. Langevin stabilization of molecular dynamics. J Chem Phys 2001;114(5):2090–8.

[50] Toukmaji AY, Board Jr JA. Ewald summation techniques in perspective: a survey. Comput Phys Commun 1996;95(2–3):73–92.
[51] Pallesen J, Wang N, Corbett KS, Wrapp D, Kirchdoerfer RN, Turner HL, et al. Immunogenicity and structures of a rationally designed prefusion MERS-CoV spike antigen. Proc Natl Acad Sci 2017;114(35):E7348–57.
[52] Yuan Y, Cao D, Zhang Y, Ma J, Qi J, Wang Q, et al. Cryo-EM structures of MERS-CoV and SARS-CoV spike glycoproteins reveal the dynamic receptor binding domains. Nat Commun 2017;8(1):15092.
[53] Vetriani C, Maeder DL, Tolliday N, Yip KS-P, Stillman TJ, Britton KL, et al. Protein thermostability above 100°C: a key role for ionic interactions. Proc Natl Acad Sci 1998;95(21):12300–5.
[54] Lam SY, Yeung RCY, Yu T-H, Sze K-H, Wong K-B. A rigidifying salt-bridge favors the activity of thermophilic enzyme at high temperatures at the expense of low-temperature activity. PLoS Biol 2011;9(3):e1001027.
[55] Elcock AH. The stability of salt bridges at high temperatures: implications for hyperthermophilic proteins11Edited by B. Honig. J Mol Biol 1998;284(2):489–502.
[56] Ge M, Xia X-Y, Pan X-M. Salt Bridges in the Hyperthermophilic Protein Ssh10b Are Resilient to Temperature Increases. J Biol Chem. 2008 November 14, 2008;283(46):31690-6.
[57] Lovell SC, Davis IW, Arendall III WB, de Bakker PIW, Word JM, Prisant MG, et al. Structure validation by Cα geometry: ϕ, ψ and Cβ deviation. Proteins Struct Funct Bioinf 2003;50(3):437–50.
[58] Moradi M, Babin V, Sagui C, Roland C. A statistical analysis of the PPII propensity of amino acid guests in proline-rich peptides. Biophys J 2011;100(4):1083–93.
[59] Matsuo K, Sakurada Y, Yonehara R, Kataoka M, Gekko K. Secondary-structure analysis of denatured proteins by vacuum-ultraviolet circular dichroism spectroscopy. Biophys J 2007;92(11):4088–96.
[60] Henderson R, Edwards RJ, Mansouri K, Janowska K, Stalls V, Gobeil SMC, et al. Controlling the SARS-CoV-2 spike glycoprotein conformatio. Nat Struct Mol Biol 2020;27(10):925–33.
[61] Hoffmann M, Kleine-Weber H, Schroeder S, Krüger N, Herrler T, Erichsen S, et al. SARS-CoV-2 cell entry depends on ACE2 and TMPRSS2 and is blocked by a clinically proven protease inhibitor. Cell 2020;181(2). 271-80.e8.
[62] Bai X, Wang Y, Song Z, Feng Y, Chen Y, Zhang D, et al. The basic properties of gold nanoparticles and their applications in tumor diagnosis and treatment. Int J Mol Sci 2020;21(7):2480.
[63] Vines JB, Yoon J-H, Ryu N-E, Lim D-J, Park H. Gold Nanoparticles for Photothermal Cancer Therapy. Frontiers in Chemistry. [Review]. 2019 2019-April-05;7(167).
[64] Schwartz-Duval AS, Konopka CJ, Moitra P, Daza EA, Srivastava I, Johnson EV, et al. Intratumoral generation of photothermal gold nanoparticles through a vectorized biomineralization of ionic gold. Nat Commun 2020;11(1):4530.
[65] Yougbaré S, Mutalik C, Krisnawati DI, Kristanto H, Jazidie A, Nuh M, et al. Nanomaterials for the photothermal killing of bacteria. Nanomaterials 2020;10(6):1123.
[66] Labouta HI, Hooshmand N, Upreti T, El-Sayed MA. Localized plasmonic photothermal therapy as a life-saving treatment paradigm for hospitalized COVID-19 patients. Plasmonics 2021.